Journal of ELECTRONIC MATERIALS, Vol. 41, No. 6, 2012
DOI: 10.1007/s11664-011-1884-6

Maximum Power Point Tracking Controller for Thermoelectric Generators with Peak Gain Control of Boost DC–DC Converters

JUNGYONG PARK[1] and SHIHO KIM[2,3]

1.—Department of Electrical Engineering, Chungbuk National University, Chungbuk 361-763, Korea. 2.—School of Integrated Technology and Yonsei Institute of Convergence Technology (YICT), Yonsei University, Songdo, Incheon 406-840, Korea. 3.—e-mail: shiho@yonsei.ac.kr

An analog maximum power point tracking (MPPT) circuit for a thermoelectric generator (TEG) is proposed. We show that the peak point of the voltage conversion gain of a boost DC–DC converter with an input voltage source having an internal resistor is the maximum power point of the TEG. The key characteristic of the proposed MPPT controller is that the duty ratio of the input clock pulse to the boost DC–DC converter shifts toward the maximum power point of the TEG by seeking the peak gain point of the boost DC–DC converters. The proposed MPPT technique provides a simple and useful analog MPPT solution, without employing digital microcontroller units.

Key words: Maximum power point tracking (MPPT), analog MPPT controller, thermoelectric generator (TEG)

INTRODUCTION

A thermoelectric generator (TEG) is a solid-state energy converter that generates electric power from the temperature difference between two hot and cold sides. Systems for energy recovery from waste heat using TEGs have recently attracted attention in areas where a considerable amount of thermal energy is wasted, such as in vehicle applications.[1–3] The voltage generated in the TEG changes dynamically over a wide range as a function of temperature. Figure 1 shows the voltage–current (V–I) characteristic of a bismuth telluride (Bi_2Te_3) thermoelectric module. As shown in Fig. 2, the equivalent circuit of a TEG can be modeled as a voltage source (V_S), which is proportional to the Seebeck coefficient and the temperature difference, with an internal resistance of R_S.[4] For maximum energy utilization, maximum power point tracking (MPPT) should be implemented to shift the operating point of a TEG toward its optimal position.

Several MPPT methods such as the perturbation and observation method, incremental conductance method, ripple correlation control method, fuzzy logic models, and neural network-based models have been proposed for implementation in photovoltaic applications.[5–11] However, these methods are not optimized for the power–current characteristics of TEGs.

A technique with seamless mode transfer MPPT[12] and an MPPT scheme for a thermoelectric battery storage system[3] have been proposed for vehicular applications of a TEG. A practical MPPT power conditioner comprising a buck-boost converter, an internal power supply, and a microcontroller for the TEG was developed to reduce the mismatch power loss and enhance the load matching ability of the TEG system.[6] These methods provide smooth transition between operating modes; however, they require a microcontroller unit to calculate the instantaneous power and peak power points.

Recently, a digital coreless MPPT tracking technique that samples the half V_S level to provide a useful analog MPPT solution, without the measurement of the input/output power or algorithmic calculation to obtain the operating points, was presented. However, the switching circuit used in the periodic half V_S sampling block, which is located between the output terminal of the TEG and the input port of the boost converter, increases the effective internal resistance of the TEG, resulting in transfer power loss.

The electrical circuit model of the TEG is a voltage source, V_S, with an internal resistance R_S that can be calculated by V_S/I_{SC},[4,13] where I_{SC} is the

(Received July 15, 2011; accepted December 21, 2011; published online January 21, 2012)

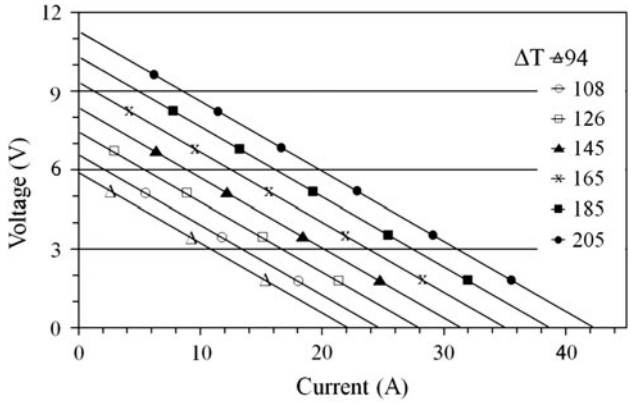

Fig. 1. Measured *V–I* characteristics of a Bi_2Te_3 thermoelectric module. The key indicates temperature difference in degrees Celsius.

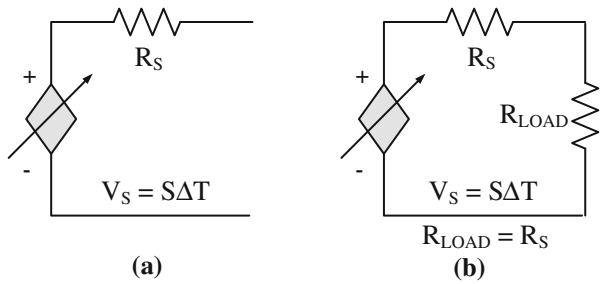

Fig. 2. (a) Equivalent model and (b) maximum power transfer condition of a TEG.

short-circuit current. The maximum power transfer condition is that R_S is equal to a load resistance R_L, as illustrated in Fig. 2b.

The corresponding ideal maximum output power P_{max} is calculated as[12,13]

$$P_{\max}|_{\mathrm{MPPT}} = \frac{V_S^2}{4R_s} = \frac{(R_S I_{SC})^2}{4}. \quad (1)$$

Despite changes in the temperature and the load resistance, the MPPT scheme tracks the maximum power point of the TEG.

While current flows in the TEG, the electrical power (Watts) as a result of Joule heating creates a temperature drop across the interface between the two plates. This diminishes the temperature difference (ΔT) across the thermoelectric material and attenuates the Seebeck voltage. In this case, the maximum power point is not simply at half the open-circuit voltage of the TEG.[14]

In this paper, we propose an analog MPPT circuit for a TEG with peak gain control of boost DC–DC converters. The key characteristic of the proposed MPPT controller is that the duty ratio of the input clock pulse to the boost DC–DC converter shifts toward the maximum power point of the TEG by seeking the peak gain point of the boost DC–DC converters.

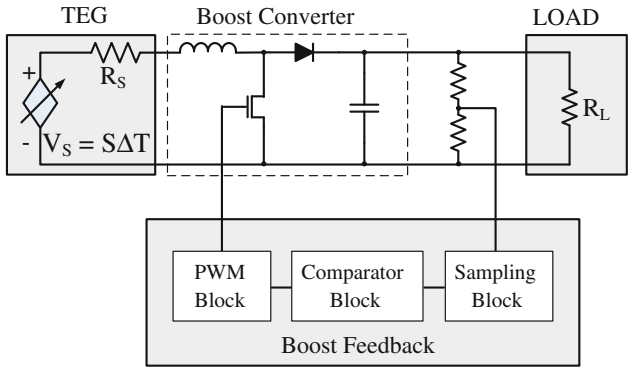

Fig. 3. Block diagram of the proposed MPPT circuit using a boost converter.

CONFIGURATION OF THE PROPOSED MPPT CIRCUIT

Figure 3 shows a block diagram of the proposed MPPT circuit composed of a boost DC–DC converter and a feedback circuit including sampling, comparator, and pulse width modulation (PWM) blocks. We consider the booster converter in the MPPT circuit, having a nonideal input voltage source with internal resistance R_S and load resistance R_L. Under the steady-state condition of the boost DC–DC converter, the average value or DC components of the inductor voltage waveform must be zero. Further, the average current that flows through an ideal capacitor must be zero, because the inductor current is supposed to have the same value at the beginning and at the end of the commutation cycle. We obtain the conversion gain and inductor current of the nonideal boost converter[15] as

$$\frac{V_{\mathrm{LOAD}}}{V_S} = \frac{1}{(1-D)} \frac{1}{\left(1 + \frac{R_S}{(1-D)^2 R_L}\right)}, \quad (2)$$

$$I_L = \frac{V_S}{(1-D)^2 R_L} \frac{1}{\left(1 + \frac{R_S}{(1-D)^2 R_L}\right)}. \quad (3)$$

The conversion gain obtained from Eq. 2 is plotted in Fig. 4 for various values of R_S/R_L as a function of the duty ratio, D. In the ideal case of a boost converter with $R_L = 0$, the voltage conversion ratio tends to infinity as D approaches 100%. However, the maximum conversion gain of the nonideal booster converter is limited by the value of the ratio R_S/R_L.[15]

The duty cycle at the peak conversion point, D_{max}, is calculated by differentiating Eq. 1 with respect to D, which yields the following relationship:

$$D_{\max} = 1 - \sqrt{\frac{R_S}{R_L}}. \quad (4)$$

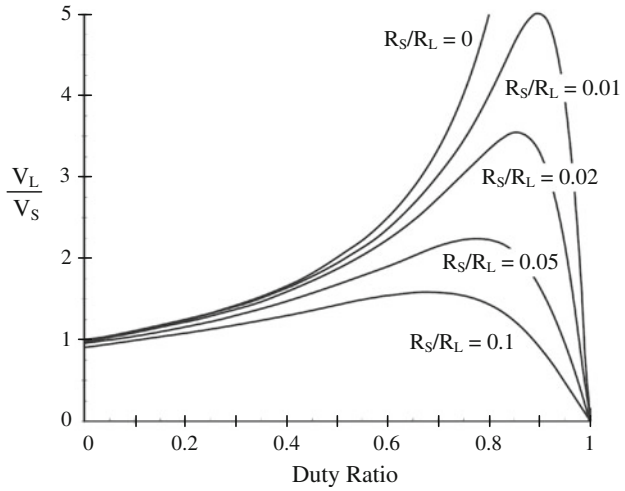

Fig. 4. Output voltage versus duty cycle for a boost converter with an input voltage source having internal resistance R_S with output load R_L.[15]

By substituting Eq. 4 into Eq. 2, we obtain the peak conversion gain as

$$\left.\frac{V_{LOAD}}{V_S}\right|_{max} = \frac{1}{2}\sqrt{\frac{R_L}{R_S}}. \quad (5)$$

The output power at the duty ratio of the maximum conversion gain, D_{max}, can be determined as

$$P_{out}|_{D_{max}} = \left.\frac{V_{LOAD}^2}{R_L}\right|_{D_{max}} = \frac{V_S^2}{4R_S} = P_{max}|_{MPPT}. \quad (6)$$

Equation 6 shows that the output power of the nonideal boost converter at D_{max} as the operating point is identical to the maximum output power of the thermoelectric module, which indicates that the duty ratio D_{max} is the operating point of the boost DC–DC converter for MPPT. Therefore, we can transfer the maximum power of the TEG to the load by tracking the duty ratio of the peak gain point of the nonideal boost DC–DC converter.

Figure 5 shows the proposed MPPT circuit with a feedback loop comprising the sampling, comparator, and PWM circuits. Signals V_{S1}, V_{S2}, and V_{LATCH} are the timing control signals for sampling and comparing the sampled load voltage. The comparator compares the sampled output voltage for every six clock pulses. The timing diagram of the proposed circuit is shown in Fig. 5c. The sampling period and the duration for comparison, T_{cycle}, can be varied depending on the transient response of the boost converter.

If the duty cycle of the input PWM pulse does not reach the D_{max} point, the comparator output becomes high because V_{S1} is greater than V_{S2}. On the other hand, if the duty cycle of the input PWM pulse passes the D_{max} point, the comparator output becomes low. The duty cycle is modulated by the

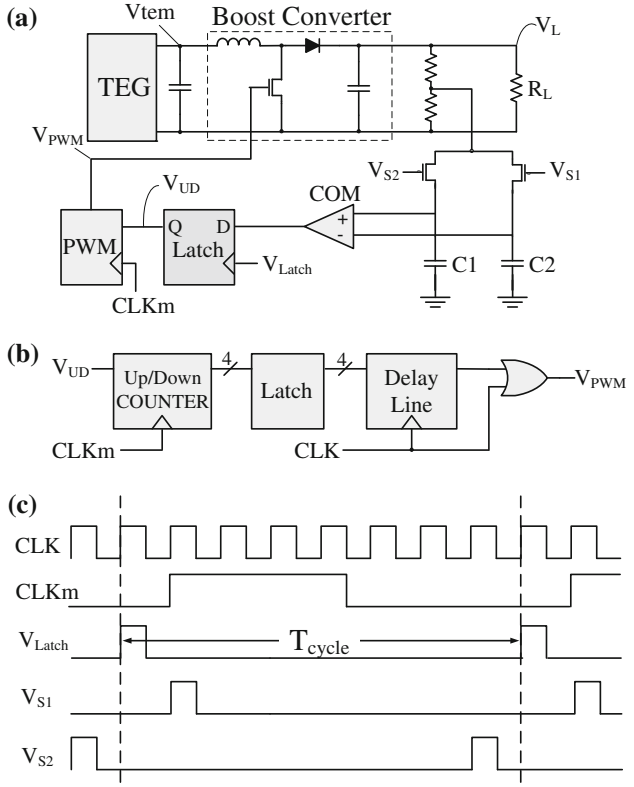

Fig. 5. Proposed MPPT circuit with feedback circuit comprising sampling, comparator, and PWM circuits. (a) Schematic diagram of the MPPT circuit. (b) Schematic diagram of the PWM block. (c) Timing diagram of operation pulse signal of comparators.

PWM block, which comprises an up/down counter and a delay line as shown in Fig. 5b. When the comparator output is high, the duty cycle increases by one step. Conversely, when the comparator output is low, the duty cycle decreases by one step. The comparator output may toggle at the maximum operating point, which could cause the duty cycle to vary around the value of D_{max}. It is essential to set the incremental value for one step increase in the duty cycle for operation of the proposed circuit within the tolerance margin at the peak voltage conversion point. Figure 6 shows the configuration of the proposed MPPT circuit with a Schmitt trigger comparator to prevent toggling of the duty cycle near the maximum power point. When the sampled output voltage is less than the input voltage window of the Schmitt trigger for two consecutive clock pulses, it holds the duty cycle of the PWM signal steady by disabling the counting operation of the up/down counter. Once the up/down counter operation is disabled, the duty ratio remains constant until the sampled voltage exceeds the input voltage window of the Schmitt trigger.

SIMULATION RESULTS AND DISCUSSION

Figure 7 shows the calculated and SPICE simulated voltage conversion ratio when the value of

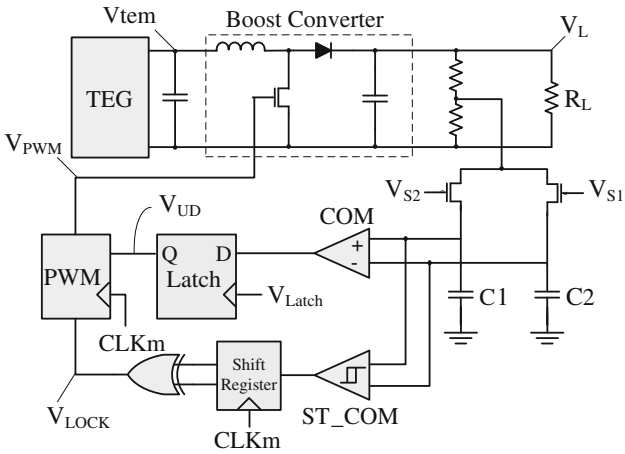

Fig. 6. Configuration of the proposed MPPT circuit with a Schmitt trigger comparator to prevent switching of the comparator output near the peak power point.

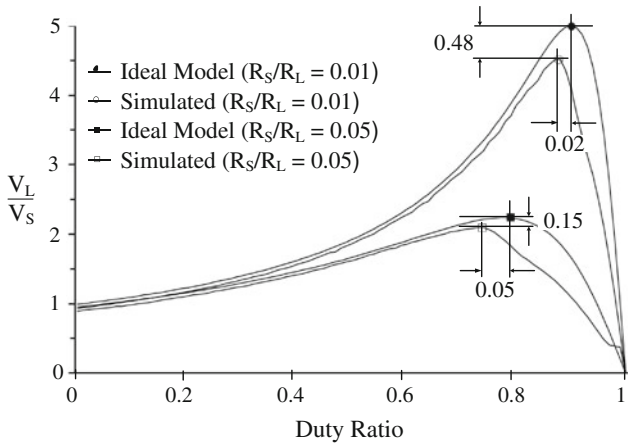

Fig. 7. Calculated ideal and simulated voltage conversion ratios for R_S/R_L equal to 0.05 and 0.01.

R_S/R_L is 0.05 and 0.01. The ideal peak conversion gain and the duty ratio of the nonideal booster converter are approximately 5.0 at duty of 90% and 2.2 at duty of 77.6% when R_S/R_L is 0.01 and 0.05, respectively. The simulated duty ratio at the peak point is approximately 73.5% and 88.6%, and the maximum difference between the simulated duty ratio and the ideal duty ratio is approximately 5%. The parasitic resistances of the NMOS transistor and the diode switch in the boost converter cause an additional reduction in the conversion gain. This reduction in the conversion gain is not accounted for in the equation for the conversion gain and the inductor current of the nonideal boost converter.

Figure 8 shows SPICE simulated voltage waveforms of the proposed MPPT circuit (V_L), PWM, and comparator output signals when the load resistance is abruptly changed from 5.2 Ω to 26 Ω with V_S fixed at 12 V. The simulated maximum output load voltage is approximately 26.5 V and 50.2 V when the

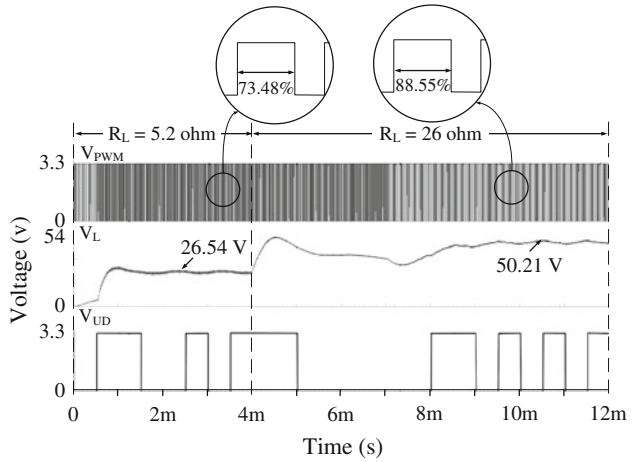

Fig. 8. Simulated voltage waveforms of the PWM output signal, V_L, and comparator output signal on abrupt change in R_L from 5.2 Ω to 26 Ω with V_S fixed at 12 V.

load resistance is 5.2 Ω and 26 Ω, respectively. The simulation results show that V_L tracks the peak conversion gain point when R_L is abruptly changed from 5.2 Ω to 26 Ω. The simulation results show that the duty ratio of the clock pulse shifts toward the maximum power point within 1.0 ms at start-up, taking approximately 5 ms when the load resistance is abruptly changed from 5.2 Ω to 26 Ω. The clock frequency of the boost converter was 50 kHz during the simulation.

A TEG with a boost-cascaded-with-buck converter configuration is commonly used for the constant-voltage battery charging mode applicable in a thermoelectric battery storage system for use in vehicles.[3,12,13] The scope of this study is limited to showing that a nonideal boost converter model is applicable to the MPPT for a TEG. If a constant-voltage charging method is required, we can modify the proposed circuit to the TEG with a boost-cascaded-with-buck converter configuration as shown in Fig. 9.

We have shown that the proposed MPPT technique with peak gain control of boost DC–DC converters provides a useful analog MPPT solution without employing digital signal processor (DSP) or microcontroller units to calculate the peak power point using iterative methods.

CONCLUSIONS

We propose an analog MPPT circuit for a TEG using peak gain control of boost DC–DC converters. The key characteristic of the proposed MPPT controller is that the duty ratio of the input clock pulse of the boost DC–DC converter shifts toward the maximum power point of the TEG by seeking the peak gain point of the boost DC–DC converters. Further, we have shown that the peak gain point of the boost DC–DC converter with an input voltage source having internal resistance R_s is the maximum power point of the TEG employing boost DC–DC converters.

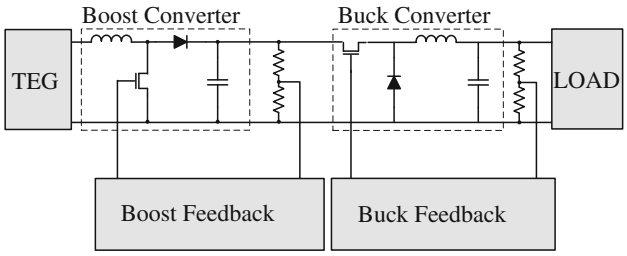

Fig. 9. Configuration of the proposed MPPT circuit with a boost-cascaded-with-buck converter.

The advantage of this method is that the analog tracking method does not employ a DSP or microcontroller unit to calculate the peak power point by iterative methods. The simulation results show that the proposed analog MPPT circuit is a potential solution for enhancing the performance of TEGs.

ACKNOWLEDGEMENT

This research was supported in part by the MKE, Korea, under the "IT Consilience Creative Program" support program supervised by the NIPA (NIPA-2010-C1515-1001-0001). The authors thank IDEC for supporting EDA tools and MPW shuttle service.

REFERENCES

1. J. Yang and F. Stabler, *J. Electron. Mater.* 38, 1245 (2009).
2. S. Kim, S. Park, S. Kim, and S. RHI, *J. Electron. Mater.* 40, 812 (2011).
3. R. Kim, J. Lai, B. York, and A. Koran, *IEEE Trans. Ind. Electron.* 56, 3709 (2009).
4. D. Mitrani, A. Tome, J. Salazar, A. Turo, M. Garcia, and J. Charvez, *IEEE Trans. Instrum. Meas.* 54, 1548 (2005).
5. I. Laird, H. Lovatt, N. Savvides, D. Lu, and V.G. Agelidis, *Proceeding of the Australasian Universities Power Engineering Conference* (AUPEC 2008), pp. 1–6.
6. H. Nagayoshi, K.Tokumisu, and T. Kajikawa, *Proceeding of the 26th International Conference on Thermoelectrics* (ICT 2007), pp. 318–321.
7. N. Femia, G. Petrone, G. Spagnuolo, and M. Vitelli, *IEEE Trans. Power Electron.* 20, 963 (2005).
8. N. Kasa, T. Iida, and L. Chen, *IEEE Trans. Ind. Electron.* 52, 1145 (2005).
9. Y.-C. Kuo, T.-J. Liang, and J.-F. Chen, *IEEE Trans. Ind. Electron.* 48, 594 (2001).
10. Y. Lim and D. Hamill, *Electron. Lett.* 36, 997 (2000).
11. T. Kottas, Y. Boutalis, and A. Karlis, *IEEE Trans. Energy Convers.* 21, 793 (2006).
12. R. Kim and J. Lai, *IEEE Trans. Power Electron.* 23, 2310 (2008).
13. S. Kim, S. Cho, N. Kim, N. Baatar, and J. Kwon, *J. Electron. Mater.* 40, 867 (2011).
14. M. Spry, *The 30th International Conference on Thermoelectrics* (ICT 2011), p 431.
15. R.W. Erickson and D. Maksimovic, *Fundamentals of Power Electronics*, 2nd ed. (Norwell: Kluwer, 2001).